

An atomic force microscopy study of DNA hairpin probes monolabelled with gold nanoparticle: Grafting and hybridization on oxide thin films

V. Lavalley, P. Chaudouët, V. Stambouli *

LMGP Laboratoire des Matériaux et du Génie Physique, INP Grenoble – Minatoc, 3 parvis Louis Néel, BP 257, 38016 Grenoble Cedex 1, France

Received 15 December 2006; accepted for publication 3 September 2007

Available online 20 September 2007

Abstract

First and original results are reported regarding the surface evolution of two kinds of oxide film after covalent grafting and hybridization of hairpin oligonucleotide probes. These hairpin probes were monolabelled with a 1.4 nm gold nanoparticle. One kind of oxide film was rough Sb doped SnO₂ oxide film and the other kind was smooth SiO₂ film. Same process of covalent grafting, involving a silanization step, was performed on both oxide surfaces. Atomic force microscopy (AFM) was used to study the evolution of each oxide surface after different steps of the process: functionalization, probe grafting and hybridization. In the case of rough SnO₂ films, a slight decrease of the roughness was observed after each step whereas in the case of smooth SiO₂ films, a maximum of roughness was obtained after probe grafting. Step height measurements of grafted probes could be performed on SiO₂ leading to an apparent thickness of around 3.7 ± 1.0 nm. After hybridization, on the granular surface of SnO₂, by coupling AFM with SEM FEG analyses, dispersed and well-resolved groups of gold nanoparticles linked to DNA duplexes could be observed. Their density varied from $6.6 \pm 0.3 \times 10^{10}$ to $2.3 \pm 0.3 \times 10^{11}$ dots cm⁻². On the contrary, on smooth SiO₂ surface, the DNA duplexes behave like a dense carpet of globular structures with a density of $2.9 \pm 0.5 \times 10^{11}$ globular structures cm⁻².

© 2007 Elsevier B.V. All rights reserved.

Keywords: DNA hairpin probes; DNA hybridization; Gold nanoparticle; AFM measurements; Oxide films

1. Introduction

DNA biochips are in high development since they have shown tremendous promise for medical research diagnosis, process monitoring in the food industry and environmental testing. They rely on the specific hybridization between single stranded DNA (ssDNA) immobilized on a surface (DNA probes) and free complementary ssDNA (DNA target) in solution. The hybridization is strongly influenced by the conformation, the density and the accessibility of the probes on the solid surface. In order to improve the sensitivity, the selectivity and the reliability of such devices, the

interface solid surface/ssDNA and the interaction between probes and targets must be characterized precisely with high resolution techniques. Indeed, the commonly used detection techniques such as fluorescence microscopy [1] and ³²P-radiolabeling experiments [2] allow global measurements over large surface area. However, these techniques cannot resolve the high lateral resolution required to characterize DNA biochips. A technique with higher lateral resolution is the atomic force microscopy (AFM) which allows obtaining a topographic image of a solid surface with a nanometric resolution. Consequently, AFM become more used to characterize single molecules in air or in solution.

However, in the field of DNA biochips, only few publications deal with AFM studies performed on DNA strands covalently grafted on biochip surfaces. Indeed, most of the

* Corresponding author.

E-mail address: Valerie.Stambouli-Sene@inpg.fr (V. Stambouli).

studies deal with long DNA molecules such as plasmid adsorbed on different substrates: sapphire [3], silicon [4], mica [5–7] or shorter double-stranded DNA (dsDNA) and linear ssDNA either physisorbed on highly oriented pyrolytic graphite (HOPG) [8] or chemisorbed on gold films [9]. By contrast, AFM studies performed on short DNA strands covalently grafted are limited. For example, such a study has been performed on SiO₂ film by Rouillat et al. [10], who investigated the organization of linear DNA strands (25 bases) after covalent grafting and hybridization. To the best of our knowledge, no publication has been reported about grafting and hybridization of hairpin DNA probes.

Hairpin probes compose a stem in which both strands are complementary and a loop. The interest of such DNA probe conformation is that these oligonucleotide sequences are very sensitive to detect one or more mismatch [11–13]. Furthermore, these hairpins can be functionalized by different elements such as gold nanoparticle, in association with a fluorescent dye, for detection by fluorescence microscopy [14]. Another interest can be provided by the use of gold nanoparticle labelled DNA: an unexpected rearrangement of the surface-confined probe-target hybrids. This rearrangement significantly enhances the quality of AFM imaging [15].

Present work shows the use of hairpin oligonucleotides modified by a 1.4 nm gold nanoparticle as probes grafted on two kinds of thin oxide films: antimony doped tin oxide (Sb doped SnO₂) film and silicon oxide (SiO₂) film. These oxide films can undergo the same process of covalent DNA probe grafting on their surface. Sb doped SnO₂ films were deposited at the laboratory using aerosol pyrolysis technique. The films were polycrystalline and exhibited a granular and rough surface [16]. As they are electrically conductive, they can be used as DNA-modified electrodes involved in electrochemical detection based biochips. Indeed, we have demonstrated their relevant and promising use for label-free electrical detection of DNA hybridization by electrochemical impedance spectroscopy [17]. In this reference, the naturally rough SnO₂ surface was modified with oligonucleotide probes exhibiting linear conformation. However, as mentioned above, a better sensitivity to detect mismatch should be expected when using hairpin probes. So, in the aim to better control the SnO₂ surface morphology when modified with gold nanoparticle labelled hairpin probes, we have investigated its evolution using AFM after different modification steps: functionalization, hairpin probe grafting and hybridization with fluorescent complementary target. In order to have a reference surface, thermally oxidized Si (SiO₂) surface was also systematically explored after each step of the process. On the contrary of SnO₂ surface, SiO₂ exhibits a smooth and featureless surface which makes it favourable to AFM study. On both materials, fluorescence measurements have been systematically performed to check hybridization process. We have presented the detailed results elsewhere [18].

2. Experimental

2.1. Thin film preparation

2.1.1. SiO₂ films

SiO₂ films were obtained from cleaned (111) Si wafers by thermal oxidization performed at 1050 °C in presence of O₂ and H₂ during 190 min. The obtained SiO₂ thickness was 460 ± 4 nm as measured using ellipsometry taking 1.46 as a refractive index. The SiO₂ film surfaces were very smooth and flat (Fig. 1a and b), exhibiting a roughness of 0.23 ± 0.01 nm (Table 1).

2.1.2. Sb doped SnO₂ films

Electrically conductive Sb doped SnO₂ thin films were deposited directly on glass substrates using the aerosol pyrolysis technique which is described elsewhere [19]. This is based on the pyrolysis of an aerosol obtained by ultra-high frequency spraying of a precursor solution on a heated substrate at atmospheric pressure.

The precursor solution was obtained by dissolving SnCl₄ · 5H₂O salt in pure methanol (solution 0.2 M) and adding a 2% volume of a 0.2 M solution of SbCl₃ salt dissolved in pure methanol (Sigma–Aldrich). The substrate temperature during deposition was kept at 420 °C. The solution consumption was about 1.6 ± 0.1 ml min⁻¹. Under these conditions, the deposition rate was about 45 nm min⁻¹. The resulting film thickness was 90 ± 10 nm as measured using ellipsometry taking 1.95 as a refractive index. The electrical resistivity of the films was 2.5 ± 0.5 × 10⁻³ Ω cm. Compared to SiO₂ film surfaces, SnO₂ (Fig. 1c and d) exhibited important roughness values, i.e., 8.21 ± 2.00 nm (Table 1), which were correlated to the high deposition rate and to the polycrystalline structure [16]. The roughness resulted in a grain agglomeration of 110 ± 20 nm.

2.2. Synthesis of oligonucleotides

The synthesis and the functionalization of the oligonucleotides (ODN) (probes and targets) were carried out by Biomérieux (France). ODN syntheses were achieved on an EXPEDITE 8900 DNA synthesizer (Applied Biosystems) using standard phosphoramidite chemistry at 1 μmol scale. All the sequences are presented in Table 2.

2.2.1. Synthesis of modified hairpin oligonucleotides probes

The 32-mers synthetic oligonucleotides were used as probe precursors. They were modified with a primary amine at their 5' end and a disulfide group at their 3' end. Selected sequence of 5'-NH₂-TTTTT GCG ATG GAT AAA CCC ACT CTA CAT CGC-SSdT-3', allowed the oligonucleotides to auto-hybridize on a stem of 6 bases to form a probe with the following characteristics: a spacer of 5 bases T, a stem of 6 base pairs and a loop of 15 bases. Fig. 2 illustrates the native conformation of the hairpin. The 3' modification of the probes was introduced via the

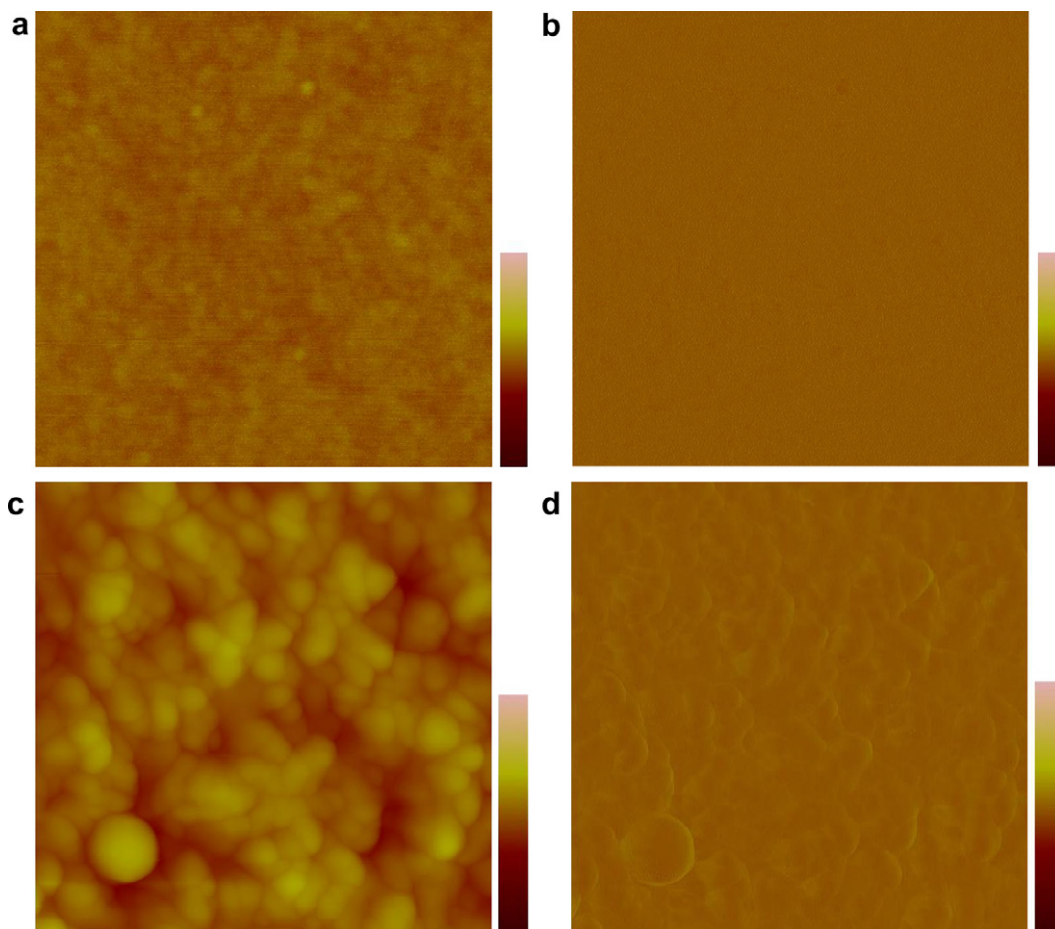


Fig. 1. AFM images (scan size $1 \mu\text{m} \times 1 \mu\text{m}$) of SiO_2 and SnO_2 bare surfaces in different modes. Respectively, (a) SiO_2 in topography or height mode (Z range 10 nm), (b) SiO_2 in phase mode (Z range 60°), (c) SnO_2 in topography mode (Z range 100 nm) and (d) SnO_2 in phase mode (Z range 90°).

Table 1
Roughness values (r.m.s.) of Sb doped SnO_2 and SiO_2 film surfaces obtained after each step of the process (scan size $1 \mu\text{m} \times 1 \mu\text{m}$)

	Sb doped $\text{SnO}_2/\text{glass}$	SiO_2/Si
Bare surface (nm)	8.21 ± 2.00	0.23 ± 0.01
Functionalized surface (APTES + glutaraldehyde) (nm)	6.52 ± 2.00	0.28 ± 0.01
Grafting of hairpin monofunctionalized by a gold nanoparticle (Probe A) (nm)	6.21 ± 2.00	0.66 ± 0.01
Hairpin (probe A) hybridization (nm)	5.93 ± 2.00	0.47 ± 0.01

3' end disulfide group, which, after reduction was further mono-functionalized either by a maleimide-gold nanoparticle (probe A, Table 2) or by a maleimide-modified fluorescein, FAM (probe B, Table 2). FAM (6 FAM, succinimidyl ester of carboxyfluorescein) and gold nanoparticles (1.4 nm

diameter nanogold[®] monomaleimide) were purchased from Molecular Probes. Because FAM and gold nanoparticle presented the same reactive monomaleimide group, the development of the mono-functionalization process of the probe was primarily investigated with FAM and then nanogold[®].

The HPLC purified 5'-NH₂-ODN-SSdT-3', was dissolved in a phosphate buffer 34 μM at pH 6.6. Then 1.5 μl of TCEP (tricarboxyl ethyl phosphine) 1 M was added to the solution of ODN to cleave the disulfide group. The solution was stirred and placed overnight at 4 $^\circ\text{C}$. Then, the solution was precipitated by centrifugation two times with 18 μl of LiClO_4 3 M, 230 μl of de-ionized water and 900 μl of acetone. Dry residue after solubilization in water was twice quantified by UV spectrometry. Measurements were taken on a 96 well Spectramax 190 (Molecular Devices) spectrophotometer at 260 nm. The cleavage of the

Table 2
Labels of the different oligonucleotides used in experiments

Name of sequences	Sequence 5' end to 3' end	5' end	3' end
Probe A	TTTTT GCG ATG GAT AAA CCC ACT CTA CAT CGC	NH ₂ C6	Nanogold [®]
Probe B	TTTTT GCG ATG GAT AAA CCC ACT CTA CAT CGC	NH ₂ C6	Fluorescein
Target A	CAGCG ATG TAG AGT GGG TTT ATC CACA	Cy3	

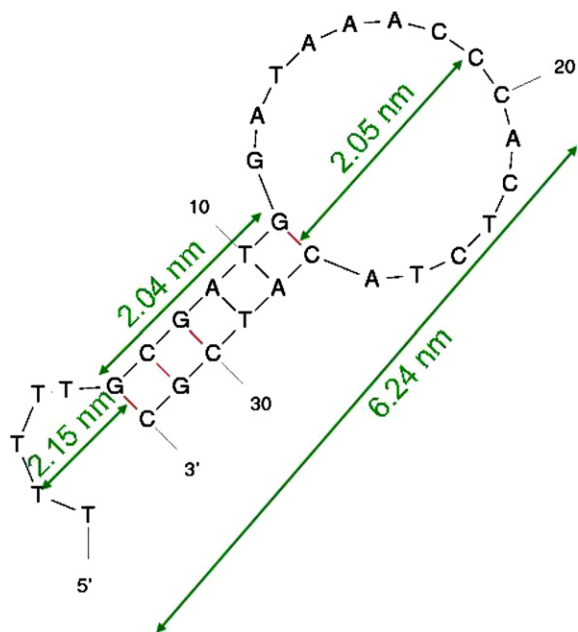


Fig. 2. Structure of the DNA hairpin probe obtained with the software mfold and calculated apparent lengths.

disulfide group was monitored by Reverse phase HPLC analyses on a Waters Alliance 2795 system using a XTERRA C18 MS 2.5 μm column 4.6 \times 50 mm (Waters), with an acetonitrile gradient from 4.5% to 8.5% in triethylammonium acetate buffer (50 mM), for 30 min at 60 $^{\circ}\text{C}$ and at 1 ml min^{-1} . A part of this crude product was subjected to mass analysis. Mass spectra for oligonucleotides were performed on a MALDI-TOF system from Bruker using 3-hydroxy picolinic acid as matrix for oligonucleotides.

The same functionalization procedure was used for FAM and nanogold[®] maleimide: 6 nmol of the maleimide compound was dissolved in 20 μl of isopropanol and 180 μl of de-ionized water. This solution was mixed with 5'NH₂-ODN-3'SH for overnight coupling reaction at 4 $^{\circ}\text{C}$. HPLC monitoring demonstrated the efficiency of the conjugation between the -SH moiety and the maleimide (95% in the case of FAM and 90% in the case of nanogold). Crude reactions were submitted to microspin purification (Amersham) in order to remove the non conjugated molecules. It is worth to note that this step is very efficient to remove the excess nanogold[®]. After UV quantification, products were used with no further purification for grafting experiments.

2.2.2. Synthesis of target

One sequence of ODN was synthesised: target A (Table 2). The ODN target sequence was complementary of the hairpin probe and labelled by a Cy3 fluorescent dye, at its 5' end in order to control the hybridization by fluorescence microscopy.

2.3. Functionalization, probe grafting and hybridization

For both SiO₂ and SnO₂ oxide films, the respective processes of bio-modification including functionalization,

probes grafting and hybridization were strictly the same. First, the surface of the oxide films was hydroxylated in a Piranha solution ($\frac{1}{3}$ H₂O₂, $\frac{2}{3}$ H₂SO₄) during 15 min to create OH groups at the surface and eliminate organic contamination. These OH groups allowed covalent bonding of a functional organosilane.

The silanization was accomplished by liquid phase deposition of a solution of silane in an organic solvent. Samples were placed for 12 h in a solution 0.5 M of 3-aminopropyl-tri-ethoxy-silane (APTES, ABCR) in 95% ethanol under shaking. After two successive rinses with ethanol (Riedel den Haen) and de-ionised water to remove unbound silane, samples were dried and heated for 3 h at 110 $^{\circ}\text{C}$.

To facilitate strong covalent binding between the NH₂ termination of APTES and the 5'NH₂ termination of the oligonucleotide, a cross linker (10% glutaraldehyde solution in H₂O, glutaraldehyde 50% purchased from Sigma–Aldrich) was applied for 90 min at room temperature. Then, the samples were rinsed with de-ionised water.

The hairpin probes were diluted in a sodium phosphate solution 0.3 M/H₂O to a concentration of 10 μM . The 10 μl of this solution was manually deposited on the surface of each sample. The samples were incubated overnight at room temperature. The probes were then reduced and stabilized using a NaBH₄ solution 0.1 M (Fluka). Then a stringent washing with an anionic detergent (0.2% sodium dodecyl sulfate) was performed to eliminate not correctly bound probes to the surface.

Hybridization was performed using a target A (Table 1). The DNA target solution was diluted in a hybridization buffer solution (NaCl: 0.5 M, phosphate buffer solution: 0.1 M, ethylenediaminetetraacetic acid or EDTA: 0.01 M at pH 5.5) to a concentrate of 1 μM . Droplets of this solution were spread ($V = 10 \mu\text{l}$) on the sample surface, covered with a hybrislip[®], and then placed into a hybridization chamber at 42 $^{\circ}\text{C}$ for 45 min. After that, samples were rinsed with SSC (saline sodium buffer concentrate, Fluka) 2 X solution, SSC 0.2 X solution and dried.

2.4. Characterization techniques

The surface topography and the roughness (in root mean-square, r.m.s.) of the thin films were explored using a Dimension 3100 Atomic Force Microscopy, AFM (Veeco Inc, Santa Barbara, CA). Measurements were performed in air in tapping mode with tip ATEC NC 10 from Nanosensors. These Si tips have a curvature tip less than 10 nm, a thickness of 4.6 μm , a length of 160 μm , a width of 45 μm , a resonance frequency between 210 and 490 kHz (nominal value: 335) and a force constant between 12 and 110 N/m (nominal value: 45). Images were collected with a resolution of 512 points per line at a scan rate of 1 Hz. Most of them were processed by flattening in order to remove the background slope, except for the image of Fig. 3a. In this case a planefit was performed to measure step height. Contrast and brightness were adjusted.

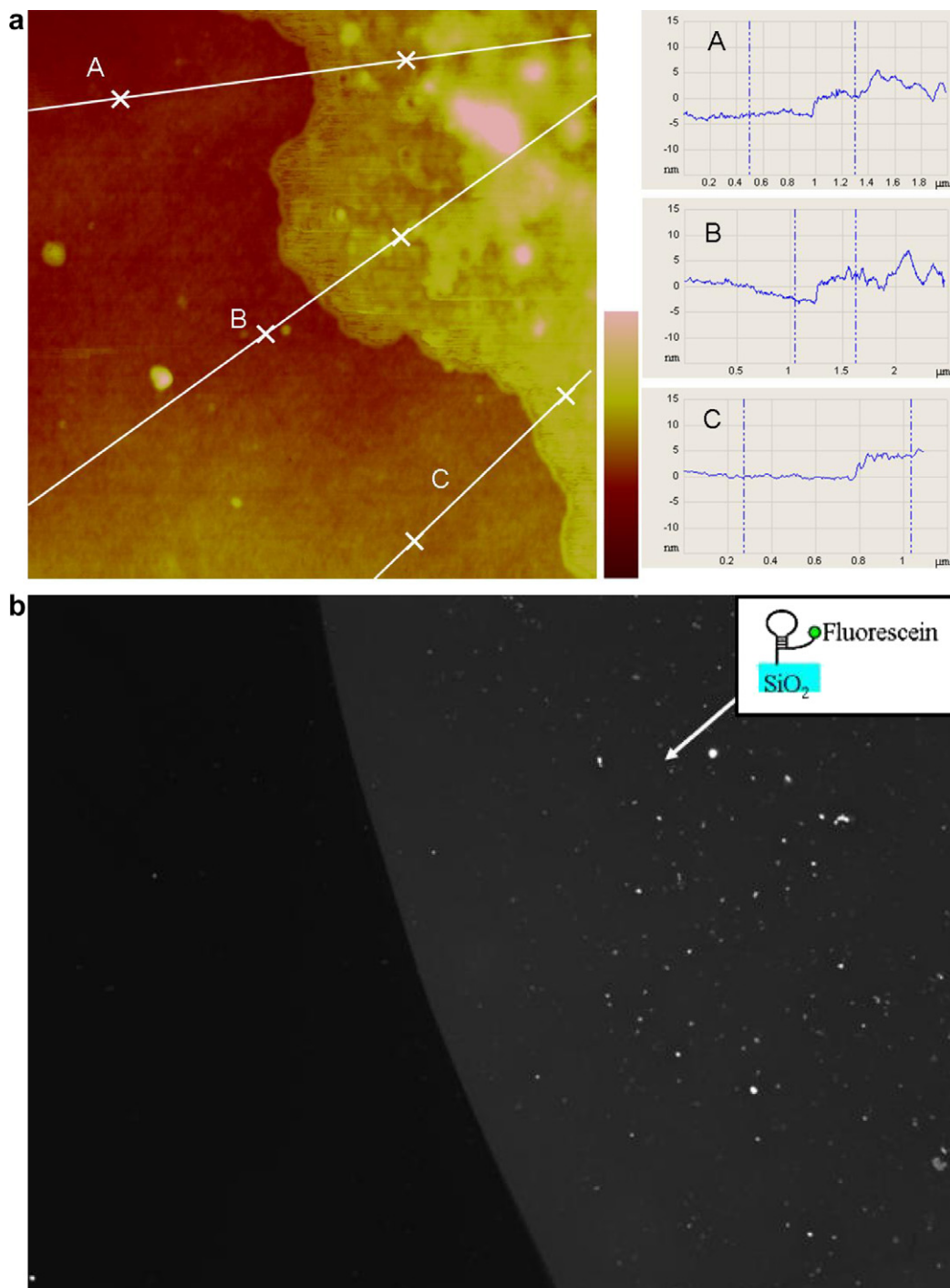


Fig. 3. (a) AFM image of near-edge of grafted fluorescein monolabelled hairpin probes, scan size $2\ \mu\text{m} \times 2\ \mu\text{m}$, obtained on SiO_2 film (Z range 20 nm). A, B, C profiles gave steps heights respectively of 3.8, 4.9 and 4.2 nm. (b) Fluorescence image of the same near-edge of grafted hairpin probes.

A scanning electron microscope equipped with a field emission gun (SEM-FEG) ZEISS Ultra was used to supplement AFM observations on SnO_2 films. This SEM-FEG, equipped with a detector in lens, collects back scattered electrons (BSE) which allow obtaining chemical contrast images. The higher is the atomic number of a considered element, the more important is the number of back scattered electrons, the brighter appears this element and enhanced is the contrast on the image. This technique

has been used essentially as to visualize gold nanoparticles.

3. Results and discussion

3.1. Control of hairpin probe grafting

AFM was used to measure the surface roughness for both oxide films – SiO_2 and Sb doped SnO_2 – at each main

step of the process: before (Fig. 1a and b) and after functionalization (silane + glutaraldehyde), then after grafting of the probes (Table 1).

For SiO₂ films, roughness slightly increased from 0.23 ± 0.01 nm before functionalization (Fig. 1a) to 0.28 ± 0.01 nm after functionalization. This process induced a smooth and homogeneous layer.

The nanogold[®] probe (probe A) grafting induced circular structures which roughened the surface as the roughness (r.m.s.) increased to 0.66 ± 0.01 nm. By comparison, this value was slightly superior to 0.55 nm obtained by Rouillat et al. [10]. In this paper, the authors observed a granular structure with oblong shape after covalent grafting of linear 25 base ssDNA on a SiO₂ film. Regarding the average height, we obtained 1.2 ± 0.2 nm which is slightly inferior to 1.5–2 nm of Rouillat et al. [10]. These weak differences can be explained by the different Nanogold[®] hairpin probe conformation. From statistical counts, the density of structures could be estimated to 2.6×10^{11} structures cm⁻² (with lateral dimensions 20–24 nm) and was also comparable to the one obtained by Rouillat et al.

On the other hand, for rough doped SnO₂ films, roughness slightly decreased from 8.21 ± 2 nm before functionalization to 6.52 ± 2 nm after functionalization. It seemed that this step induced a smoothing of the surface reducing the gap between the holes and the tops. Then nanogold[®] probe grafting did not induced significant roughness difference (Table 1).

From AFM study of a near-edge of grafting area, we have attempted to measure the height or apparent thickness of grafted hairpins on oxide surface. Such experiments could only be performed on the flat SiO₂ film surface (Fig. 3a) modified with fluorescein functionalised probes (probe B, Table 2). The use of fluorescein was justified in order to check the grafting efficiency by fluorescence microscopy (Fig. 3b). From Fig. 3a, several information could be drawn. On the left side of the figure, the SiO₂ film covered by the functionalization layers (APTES and glutaraldehyde) could be easily identified due to weak roughness and homogeneous aspect. In contrast, the upper area with higher roughness located on the right side corresponded to grafted probes. This area revealed two different parts: a thin layer of covalently bound hairpin probes covered by an inhomogeneous thicker layer located mainly in the top right of the image. The origin of this thicker layer was not clearly explained. It could be due to some adsorbed hairpin probes on top of the thin layer. A less probable explanation could be provided by some residual salts. A response could be given by collecting these images in liquid under buffer conditions. This observation emphasized the importance of the rinsing procedure after hairpin probe grafting. Despite, we measured the thickness of the layer of interest, i.e., covalently bound probes. Thickness values were ranging from 0.7 nm to 4.9 nm (examples are shown in Fig 3a, profiles A, B and C), the average height being 3.7 ± 1.0 nm. To confirm that the step height corresponded to DNA material, a counter experience was performed. A

drop containing only the grafting buffer (sodium phosphate solution) without DNA probe was deposited. The AFM scans performed all along the drop edge showed no height difference between external and internal areas of the drop. Only some residual salts contributed to roughen locally the surface.

A theoretical value of the whole height of the hairpin probe could be calculated. As shown in Fig. 2, the stem was constituted of 6 hybridized base pairs which can take the structure of a double helix of DNA. According to Tinland et al. [20], the base–base length is 0.43 nm in a ssDNA and 0.34 nm in a dsDNA. Consequently, the stem is about 2.04 nm length. The length of the spacer T-T-T-T-T is about 2.15 nm. Regarding the loop, if we consider the 15 bases as a linear single strand DNA, the loop length is about 6.45 nm which can be considered as its perimeter. The theoretical diameter *D* of the loop and so its apparent height in the hairpin, is about 2.05 nm. On the whole, the total apparent height of the hairpin is about 6.24 nm. By comparison, this value could be attributed to the length of a linear ssDNA of 14 or 15 bases.

This calculated value was approximately twice than the experimental one measured by AFM (Fig. 3a). This could be explained by the fact that the measurements were performed in air and not in liquid. As a consequence, these hairpins could be tilted towards the surface with a tilt angle ranging from 38° to 59° as deduced from experimental height. Equally, the low experimental height value could also be explained by the interaction between the tip and the DNA molecules at the surface of the thin films. This interaction could induce some flattening of the DNA molecules. As a result, lower heights than expected were often measured [6,21].

As mentioned before, few publications have reported AFM studies of single strand DNA grafted on a substrate. Guiducci et al. [9] have studied chemisorbed linear ssDNA (30 bases) on a gold surface via gold–sulfur bonds. The authors used the technique named “nanoshaving”, i.e., an AFM probe can be used to scrape off the oligonucleotide layer by applying a force higher than the oligonucleotides adhesion on the surface. Using this technique, they found that ssDNA were not laid on the surface but they were stood up or tilted. They found an apparent thickness of ssDNA layer of 2 nm. Using a similar process to immobilize ssDNA (15 bases) on a gold surface, Legay et al. [22] have measured a height of 3.5 nm. This value could be compared to our experimental value as our hairpin height is similar to the one of a linear ssDNA of 14 or 15 bases. As for us, the experimental value is twice smaller than the calculated value according to Tinland et al. [20]. This shows the difficulty to measure a real value of the height of a ssDNA grafted on a solid substrate.

3.2. Study of DNA hybridization

During the hybridization, the hairpin probes unfolded and hybridized with the complementary Cy3 labelled

ssDNA target A (Table 2). Hybridization on both oxide films was confirmed by fluorescence microscopy as shown in a recently published paper [18] where specific phenomena of Cy3 quenching by the close gold nanoparticle are detailed. For both kinds of oxide films, we have studied the surface morphology obtained after hybridization of each kind of hairpin probe, especially in the case of nanogold[®] labelled probe (probe A). Results are reported in Table 1.

3.2.1. DNA hybridization on SiO₂ films

Whatever the hairpin probe, the roughness (r.m.s.) decreased after hybridization. In the case of nanogold[®] labelled probes (probe A), an homogeneous field of globular structures was observed on the surface (Fig. 4a). The roughness was found to be 0.47 ± 0.01 nm. The globular structures (Fig. 4a) exhibited nanometric dimensions of typically 1.3 ± 0.2 nm height and 20.8 ± 2.0 nm mean width. Compared with the calculated height of 12.3 nm (according to Tinland et al. [20]) for the duplex molecule without the contribution of the nanogold[®], the measured height was very small. This could be explained by a high DNA duplex density on the surface of the SiO₂ film. The DNA duplexes behaved as a homogeneous “carpet” with molecules very close to each other. As the tip curvature is around 10 nm and the resolution is in the same order, one molecule (2 nm diameter) could not be individualised by the tip. The tip only scanned the top of the duplexes without crossing the whole thickness of the DNA carpet. A statistical count could be performed and provided a density of $2.9 \pm 0.5 \times 10^{11}$ globular structures cm⁻². It was impossible to know how many DNA duplexes were included in one globular structure.

The results were confirmed from the corresponding phase image (Fig. 4b). Indeed, a significant advantage of tapping mode AFM compared with contact mode AFM, is the ability of using the changes in phase angle of the AFM cantilever probe for producing a second image: the

phase image. The phase image is recorded simultaneously with the topographic image of the surface, and represents the difference between the oscillation of the cantilever and its true response at surface contact. The reference phase is considered the free oscillation phase of the AFM cantilever, far away from the surface. During the scanning of the sample, changes in phase contrast depend not only on topography changes, but also on the adhesion, elasticity and viscoelastic properties of the surface. The modifications in the phase angle are correlated with different damping produced by different areas of the sample. Frequently, the phase images show an improved contrast compared with the corresponding DNA topographical image. As the gold nanoparticles presented mechanical and morphological properties different from those of DNA or thin film, we could expect a contrast image showing the presence of gold nanoparticles in the case of the hybridization performed with the nanogold[®] labelled probes. Fig. 4b showed a homogeneous field of globular structures as on Fig. 4a with the same characteristics of height and width.

3.2.2. DNA hybridization on SnO₂ films

The large grain structure observed on the bare SnO₂ surface (Fig. 1b) was remained at each step of the process. Whatever the kind of grafted probe, the hybridization induced a slight decrease of the roughness. In the case of nanogold[®] labelled probes (probe A), no globular structure was observed (Fig. 5a) as on SiO₂ films (Fig. 4a). Interestingly, the phase image (Fig. 5b) showed the presence of distinct nanodots dispersed on the SnO₂ surface.

These nanodots could be individualised and could be better distinguished by the AFM tip as they were dispersed on a granular surface, contrary to the smooth SiO₂ surface with a homogeneous “carpet” of DNA. Dimensions of these nanodots could be measured in terms of width but their width was more dispersed compared to the width of globular structures on SiO₂. Indeed, the smallest nanodots were 8.0 nm width whereas the biggest could measure

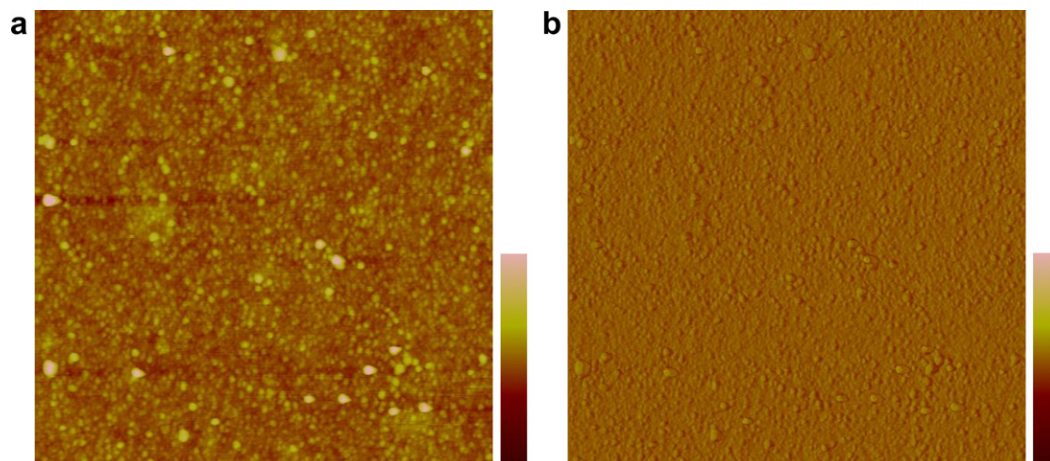


Fig. 4. AFM images (scan size $1 \mu\text{m} \times 1 \mu\text{m}$) obtained on SiO₂ film after hybridization of covalently grafted nanogold[®] labelled probes: (a) topography mode or height image (Z range 10 nm) and (b) phase image (Z range 60°).

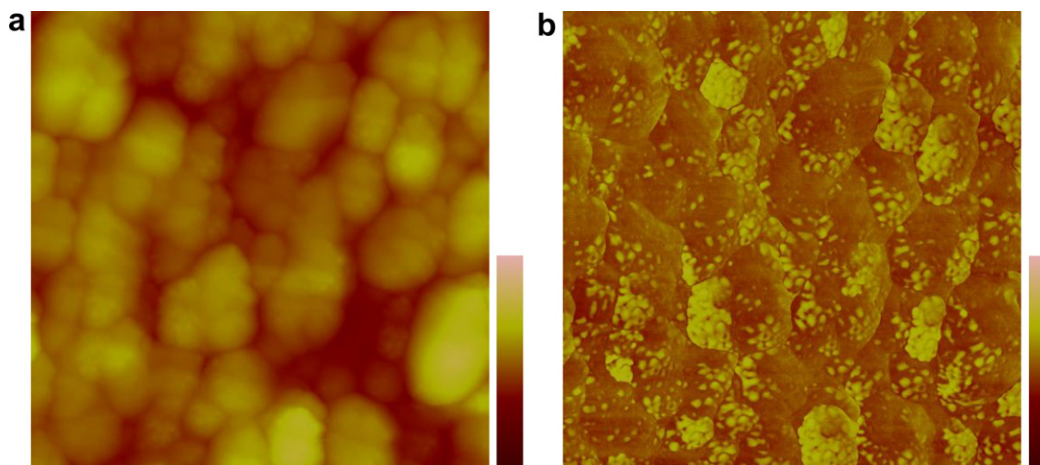


Fig. 5. AFM images (scan size $1\ \mu\text{m} \times 1\ \mu\text{m}$) obtained on SnO_2 film after hybridization of covalently grafted nanogold[®] labelled probes: (a) topography mode or height image (Z range 100 nm) and (b) phase image (Z range 90°).

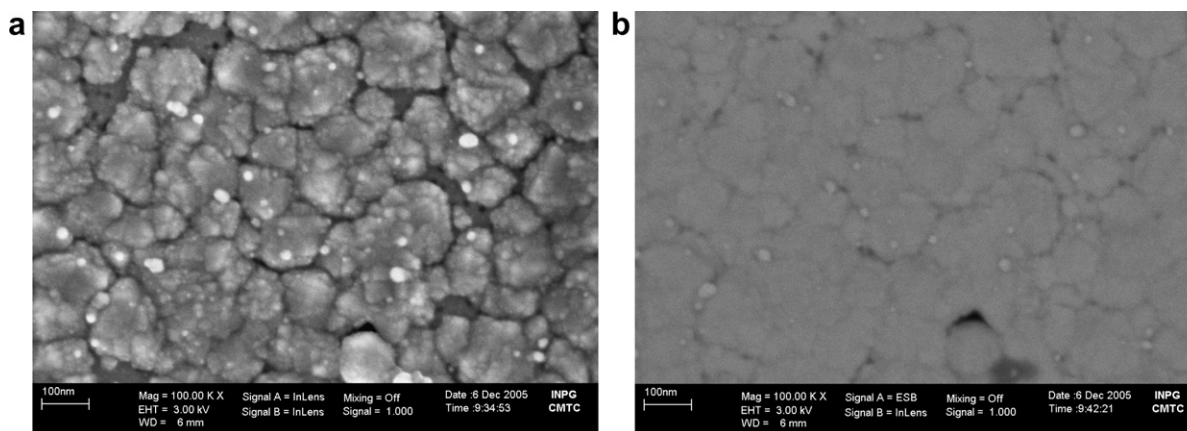


Fig. 6. SEM-FEG images obtained with (a) secondary electrons and (b) with back scattered electron (BSE) after hybridization of nanogold[®] labelled probes covalently grafted on SnO_2 film. The brightest islands were gold nanoparticles.

60.0 nm width. The most of the nanodots measured between 16.0 and 20.0 nm width. The measured width was higher than the expected value of around 2 nm, as already observed for SiO_2 . It seemed that the DNA duplexes with their nanogold[®] tend to group together themselves. A statistical count on several samples provided a density ranging from $6.6 \pm 0.5 \times 10^{10}$ (Fig. 5b) to $2.9 \pm 0.5 \times 10^{11}$ nanodots cm^{-2} . These results showed the inhomogeneous location of the hairpin probes and consequently of the duplexes on a rough surface compared to a flat surface as SiO_2 .

To confirm that these nanodots corresponded to DNA duplexes with gold nanoparticles, SEM-FEG analyses were performed. On the secondary electron image (Fig. 6a), the large grain structure of SnO_2 surface was easily observed with small white dots of different sizes. To check that these dots could be attributed to groups of nanogold[®] particles, a chemical contrast image with back scattered electrons was performed (Fig. 6b). Small and bright structures were obtained which perfectly corresponded to the white dots in

Fig. 6a. These structures, characterized by an atomic number superior to the one of SnO_2 , were attributed to groups of gold nanoparticles. It is to be noted that the resolution limit of the apparatus when using BSE mode is poorer. For this reason, dots were less resolved than in secondary electron mode so the smallest dots could not be observed. This confirmed that groups including several DNA duplexes were “dispersed” on the rough SnO_2 surface and did not behave like a dense carpet as on the smooth SiO_2 surface. One advantage for an AFM exploration of a rough and developed surface like the SnO_2 surface was the given possibility to better individualise the groups of DNA duplexes.

4. Conclusions

Hairpin oligonucleotide probes monofunctionalized either by a 1.4 nm gold nanoparticle or a fluorescein dye were grafted on two different oxide film surfaces: SiO_2 and Sb doped SnO_2 . Each step of the modification process was studied by AFM.

In the case of rough SnO₂ films, a slight decrease of the roughness was observed after each step of the modification process. In the case of smooth SiO₂ films, a roughness evolution has been evidenced with a maximum of roughness obtained after the grafting of hairpin probes. From step height measurements performed on SiO₂, an apparent thickness of grafted hairpin probes could be estimated to 3.7 ± 1.0 nm. After hybridization of hairpins, the coupling of AFM in phase mode with SEM-FEG analyses allowed to show well-resolved groups of several gold nanoparticle-DNA duplexes which are dispersed on the rough SnO₂ film whereas the DNA duplexes behave like a dense carpet of globular structures on the smooth SiO₂ film.

Acknowledgments

The facility for depositing SiO₂ films and performing fluorescence measurements was provided at the biotechnology platform of the Centre Interuniversitaire de Micro-Electronique (CIME) (Grenoble).

The monofunctionalization of the hairpin probes by a fluorescein or a gold nanoparticle was provided at Apibio (Biomérieux, Grenoble). Thanks to A. Laurent for his helpful devices.

References

- [1] Stephen P.A. Fodor, *Science* 277 (1997) 393.
- [2] T.M. Herne, M.J. Tarlov, *J. Am. Chem. Soc.* 119 (1997) 8916.
- [3] K. Yoshida, M. Yoshimoto, K. Sasaki, T. Ohnishi, T. Ushiki, J. Hitomi, S. Yamamoto, M. Sigeno, *Biophys. J.* 74 (1998) 654.
- [4] H.G. Hansma, I. Revenko, K. Kim, D.E. Laney, *Nucl. Acids Res.* 24 (1996) 713.
- [5] T. Thundat, R.J. Warmack, D.P. Allison, L.A. Bottomley, A.J. Lourenco, T.L. Ferrell, *J. Vac. Technol. A* 10 (1992) 630.
- [6] Y.L. Lyubchenko, P.I. Oden, D. Lampner, S.M. Lindsay, K.A. Dunker, *Nucl. Acids Res.* 21 (1993) 1117.
- [7] H.G. Hansma, R. Golan, W. Hsieh, C.P. Lollo, P. Mullen-Ley, D. Kwok, *Nucl. Acids Res.* 26 (1998) 2481.
- [8] A.M. Oliveira Brett, A.M. Chiorcea Paquim, *Bioelectrochemistry* 66 (2005) 117.
- [9] C. Guiducci, C. Stagni, G. Zuccheri, A. Bogliolo, L. Benini, B. Samori, B. Riccò, *Biosensor. Bioelectr.* 19 (2004) 781.
- [10] M.H. Rouillat, V. Dugas, J.R. Martin, M. Phaner-Goutorbe, *Appl. Surf. Sci.* 252 (2005) 1765.
- [11] T. Jun Huang, M. Liu, L.D. Knight, W.W. Grody, J.F. Miller, C.M. Ho, *Nucl. Acids Res.* 30 (2002) e55.
- [12] Y. Mao, C. Luo, Q. Ouyang, *Nucl. Acids Res.* 31 (2003) e108.
- [13] M. Steichen, C. Buess-Herman, *Electrochem. Commun.* 7 (2005) 416.
- [14] B. Dubertret, M. Calame, A.J. Libchaber, *Nat. Biotechnol.* 19 (2001) 365.
- [15] Shubo Han, Jianqiao Lin, Feimeng Zhou, R.L. Vellanoweth, *Biochem. Biophys. Res. Commun.* 279 (2000) 265.
- [16] V. Stambouli, M. Labeau, I. Matko, B. Chenevier, O. Renault, C. Guiducci, P. Chaudouët, H. Roussel, D. Nibkin, E. Dupuis, *Sensor. Actuator. B* 113 (2006) 1025.
- [17] V. Stambouli, A. Zebda, E. Appert, C. Guiducci, M. Labeau, J.P. Diard, B. Le Gorrec, N. Brack, P.J. Pigram, *Electrochim. Acta* 51 (24) (2006) 5206.
- [18] V. Lavalley, A. Laurent, A. Zebda, J.E. Mendez, V. Stambouli, *Sensor. Actuator. B* 124 (2007) 564.
- [19] M. Labeau, V. Redoux, D. Dhahri, J.C. Joubert, *Thin Solid Films* 136 (1986) 257.
- [20] B. Tinland, A. Pluen, J. Sturm, G. Weill, *Macromolecules* 30 (1997) 5763.
- [21] F. Moreno-Herrero, J. Colchero, A.M. Baró, *Ultramicroscopy* 96 (2003) 167.
- [22] G. Legay, E. Finot, R. Meunier-Prest, M. Cherkaoui-Malki, N. Latruffe, A. Dereux, *Biosensor. Bioelectr.* 21 (2005) 627.